ARTICLE IN PRESS

Computer Physics Communications ▮ (▮▮▮▮) ▮▮▮–▮▮▮

Contents lists available at ScienceDirect

Computer Physics Communications

journal homepage: www.elsevier.com/locate/cpc

PIC/MCC simulation of capacitively coupled discharges: Effect of particle management and integration

Anbang Sun *, Markus M. Becker, Detlef Loffhagen

Leibniz Institute for Plasma Science and Technology (INP Greifswald), Felix-Hausdorff-Str. 2, 17489 Greifswald, Germany

ARTICLE INFO

Article history:
Received 26 August 2015
Received in revised form
19 March 2016
Accepted 9 May 2016
Available online xxxx

Keywords:
PIC/MCC simulation
Capacitively coupled radio frequency discharge
Benchmark
Adaptive particle management

ABSTRACT

A PIC/MCC simulation model for the analysis of low-temperature discharge plasmas is represented which takes the common leapfrog and the velocity Verlet algorithm for the particle integration, adaptive particle management as well as parallel computing using MPI into account. Main features of the model including the impact of super particle numbers, adaptive particle management and the time step size for the different integration methods are represented. The investigations are performed for low-pressure capacitively coupled radio frequency discharges in helium and argon. Besides a code verification by comparison with benchmark simulation results in helium it is shown that an adaptive particle management is particularly suitable for the simulation of discharges at elevated pressures where boundary effects and processes in the sheath regions are important. Furthermore, it is pointed out that the velocity Verlet integration scheme allows to speed up the PIC/MCC simulations compared to the leapfrog method because it makes the use of larger time steps at the same accuracy possible.

1. Introduction

Besides experimental diagnostics, numerical modelling and simulation attract increasing attention for understanding the physics of low-temperature plasma discharges, because they are cost-effective and are able to explore properties of the plasma that are difficult to measure like the spatiotemporal evolution of plasma density, flux, energy and so on. Particle-in-Cell/Monte Carlo Collision (PIC/MCC) simulation provides a kinetic description of the plasma based on first principles. Thus, it reflects precisely the motion of charged particles and has been extensively utilized for the simulation of low-temperature plasmas [1,2]. However, high computational demand is the main drawback of such particle models, since the motion of millions of particles and the electric forces acting on the particles have to be updated at every time step during simulations.

Typically, the most critical task for particle code developers consists of reducing the computational time and increasing the efficiency of the code. Researchers use different ways to overcome the above mentioned drawback. For instance, they use adaptive particle weight [3–6], variable time step for different charged species [7,8], explicit or implicit particle integration methods [9–11] and parallelization [7,12–14]. Although the efficiency of a particle code is important, one has to be aware that the priority should be to ensure its correctness and accuracy.

The aim of the paper is to present a reliable spatially one-dimensional, three velocity coordinates (1d3v) PIC/MCC model for the simulation of low-temperature discharge plasmas, where capacitively coupled radio frequency (CCRF) discharges are considered here. The present code is extended from a previous model for streamer simulations [15]. While the previous model considered only electrons as particles and ions were immobile on the short time scale of interest of streamer discharges, both electrons and ions are followed as particles in the present code and adaptive particle management (APM) for super particles and message passing interface (MPI) computing are adapted. Furthermore, two different methods for integrating Newton's equations of motion are included. In addition to the frequently used explicit leapfrog scheme [9,16], the velocity Verlet scheme [17] is implemented. We verify the code by comparing it to a CCRF discharge benchmark established by Turner et al. [18]. Then, we check carefully how the super particle numbers per cell in the adaptive particle management method, different particle integration methods and the time step size influence the accuracy of simulations.

It is worth to mention that CCRF discharges have been widely used for plasma etching, thin film deposition in the microelectronic and semiconductor industries [19–21] as well as for surface treatment in plasma medicine [22]. In general, non-Maxwellian electron energy distribution functions (EEDF) are to be expected

* Corresponding author.
E-mail address: an-bang.sun@inp-greifswald.de (A. Sun).

http://dx.doi.org/10.1016/j.cpc.2016.05.003
0010-4655/

in low-pressure CCRF discharges [19] as, e.g., measured by Godyak et al. [23,24] in argon and helium gases. Furthermore, collisionless heating plays an important role in low pressure CCRF discharges [25]. Thus, a kinetic description of the plasma is required and many groups have developed PIC/MCC models to investigate the physical characteristics of CCRF discharges. For instance, Vahedi et al. [26] used a PIC/MCC model to produce the same EEDF as measured by Godyak et al. [24] in argon. Matyash et al. [1] applied their PIC code for understanding basic physics phenomena in different low-temperature plasmas, for instance, radio frequency discharge in oxygen [27,28], electrostatic ion thrusters [29] and negative ion sources [1,30]. A self-developed 1d3v PIC-MCC code was used to study the electron heating and ionization dynamics in CCRF atmospheric pressure microplasmas operated in helium [13]. Similarly, Iza et al. [31] used 'XPDP1' [32] to detect the non-equilibrium characteristic of electron energy probability function in the radio frequency atmospheric pressure helium microdischarges. The spatially one-dimensional, object-oriented PIC code 'oopd1' was realized to investigate the CCRF discharge in oxygen [33] and chlorine [34], where relatively complete reaction sets between charge particles and the background gas are collected. The 'PHOENIX1D' code was developed to study the electrical asymmetric effect [35], voltage waveform [36], electron heating [37] and secondary electron asymmetry effect [38] in CCRF discharges in different gases and at different pressures. Effects of fast atoms and energy-dependent SEE [39], the influence of the driving frequency on the electron heating [40] and on the electric asymmetry [41] were investigated by means of the PIC code introduced in [2]. Despite there is a large number of particle simulations on CCRF discharges and inductively coupled plasma reactors using different codes developed by different research groups, the verification of the code is always a critical process which was sometimes not performed.

The paper is organized as follows. A detailed introduction of our 1d3v PIC/MCC approach is present in Section 2. The code is verified by comparison with benchmark simulation results for low-pressure CCRF discharges in helium of Turner et al. [18] in Section 3. In Section 4, we explore the influence of different super particle numbers per cell in the adaptive particle management method and the convergence behaviour of the results with respect to the time step size using the explicit leapfrog and velocity Verlet integration method. In addition, simulations in argon are performed to further test the applicability of the model and to proof the generality of the drawn conclusions. Finally, the results are summarized in Section 5.

2. Simulation approach

We perform simulations using a 1d3v particle model of the PIC/MCC type, where our simulations are in an electrostatic regime and the action of a magnetic field is neglected. A general process of the PIC simulation runs as follows. A certain amount of particles is initialized in the domain under consideration. The velocities and positions of these particles are updated by integrating the equations of motion. Macroscopic quantities like charge density are calculated at the grid points by mapping individual particles. The electric field at the grid points is computed by solving Poisson's equation. Then, the forces acting on the particles are interpolated back to the particles from the grid points. Particles reaching the spatial borders of the discharge region considered can e.g. be absorbed or reflected at the boundaries and the corresponding boundary effects are treated after updating the velocities and positions of particles. If MCC is added, collisions are treated afterwards.

2.1. Particle integration, accuracy and stability

In common, particle integration consumes most of the computation time in PIC simulations because all particles have to be traced separately at every time step. In the present model, electrons and ions are traced as particles that can collide with neutral background gas particles. Its extension to account for the motion of e.g. excited neutral gas particles is immediately possible.

In order to simulate gas discharge plasmas, the explicit leapfrog scheme has commonly been used as e.g. in the recent benchmark simulation studies of Turner et al. [18]. An alternative particle integration method is the velocity Verlet algorithm [17], which has recently been employed for glow discharge plasma simulations in [7]. These two integration methods are also customary in molecular dynamics simulations [42].

We have implemented both these methods into the present model and deviations induced by them are discussed below. The flowchart of our PIC/MCC simulations is shown in Fig. 1.

The leapfrog scheme calculates the velocities $\vec{v}$ and the positions $\vec{x}$ of particles with an offset in time by $\Delta t/2$, i.e., half the time step Δt, according to

$$\vec{v}_{k+1/2} = \vec{v}_{k-1/2} + \vec{a}_k \Delta t, \tag{1}$$

$$\vec{x}_{k+1} = \vec{x}_k + \vec{v}_{k+1/2} \Delta t. \tag{2}$$

Here $\vec{v}_j$ with $j = k-1/2,\ k+1/2$ and $\vec{x}_j$ with $j = k,\ k+1$ are the velocity and position at the time $t_j = t_0 + j\Delta t$ with the initial time t_0, respectively, $\vec{a}_k = q\vec{E}_k/m$ is the acceleration of the particle with charge q and mass m and $\vec{E}_k$ denotes the electric field at t_k acting on the particle.

The velocity Verlet scheme is quite similar to the leapfrog integration method, except that the velocity and position are calculated at the same time t_{k+1} according to

$$\vec{x}_{k+1} = \vec{x}_k + \vec{v}_k \Delta t + \frac{1}{2}\vec{a}_k \Delta t^2, \tag{3}$$

$$\vec{v}_{k+1} = \vec{v}_k + \frac{1}{2}(\vec{a}_k + \vec{a}_{k+1})\Delta t, \tag{4}$$

where at first the position and then the velocity is determined. Notice that the acceleration a_{k+1} at the time t_{k+1} is needed for the velocity Verlet scheme which can be directly calculated from the new position $\vec{x}_{k+1}$ of all particles solving Poisson's equation (cf. Fig. 1(b)). The solution of the Poisson equation is done using a standard second-order finite difference approach on an equidistant spatial grid.

Typically, several restrictions have to be considered, in order to ensure the accuracy and stability for such explicit particle integration methods [9,16,18]. The mesh size Δx should be of the same order as the Debye length $\lambda_D = (\varepsilon_0 T_e/en_e)^{1/2}$, where ε_0 is the permittivity of free space, T_e is the electron temperature and n_e is the density of electrons with charge $-e$ and mass m_e. The time step Δt should resolve the electron plasma frequency $\omega_e = (e^2 n_e/\varepsilon_0 m_e)^{1/2}$ and satisfy the Courant–Friedrichs–Lewy (CFL) condition [43] $\Delta t \leq \Delta x/v_{max}$, where v_{max} is the maximum velocity magnitude of the particles. In addition, Δt has to resolve $\nu_{max}\Delta t \ll 1$ to ensure the accuracy of null collisions, where ν_{max} is the maximum collision frequency of the particles.

2.2. Adaptive particle management

As the number of particles in a discharge plasma is too large to be traced individually, super particles have to be used where one super particle represents many physical particles. Here, one has to keep in mind that if the weight of super particles is high, it can induce fluctuation, gas heating or numerical errors [25,7].

Please cite this article in press as: A. Sun, et al., PIC/MCC simulation of capacitively coupled discharges: Effect of particle management and integration, Computer Physics Communications (2016), http://dx.doi.org/10.1016/j.cpc.2016.05.003

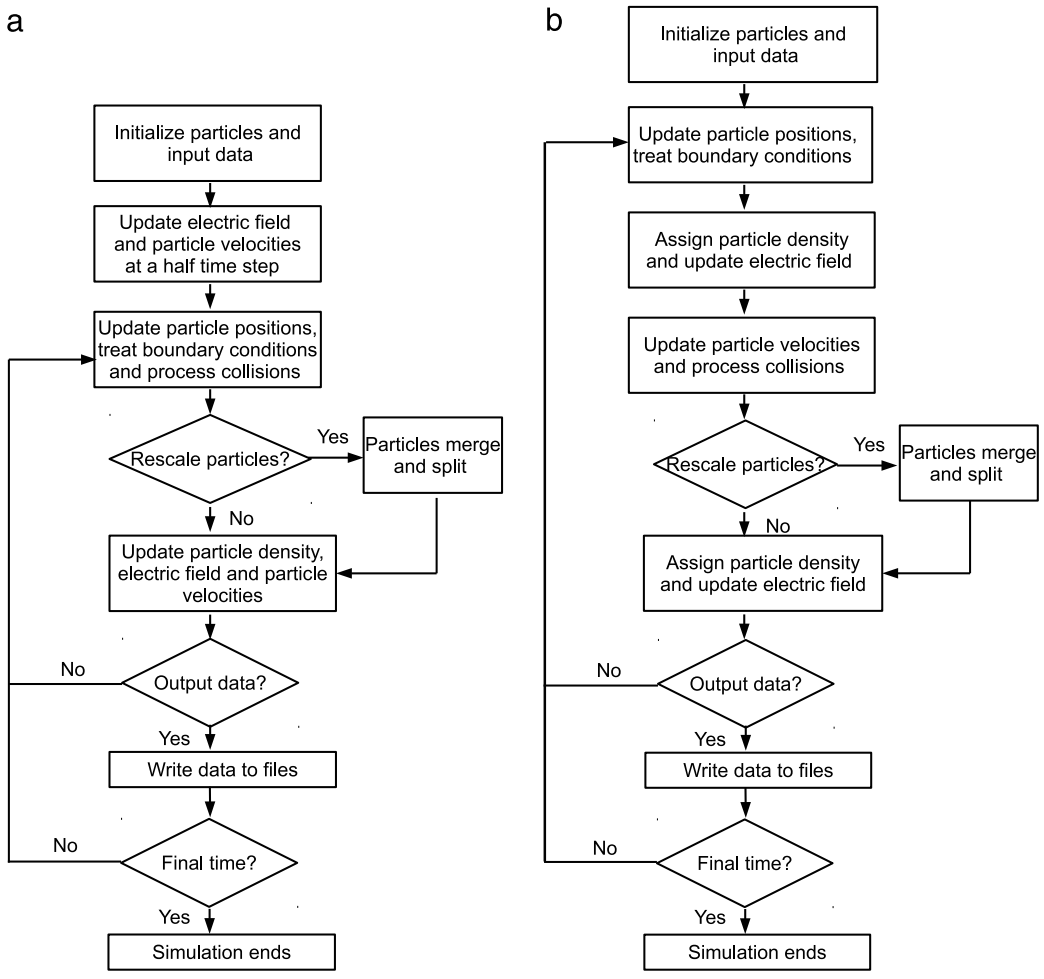

Fig. 1. Flowchart of the PIC/MCC simulation using the leapfrog scheme (a) and the velocity Verlet scheme (b).

In the present model, we use an adaptive particle management technique for adjusting the weight of particles. According to [6], a k–d tree algorithm is used to sort particles that can merge or split. We note that a k–d tree is a space partitioning data structure for organizing points in a k-dimensional space. The processes of management of particles of type s in the cell i with space and velocity coordinates $\vec{x}_i$ and $\vec{v}_i$ and weights w_i are as follows:

1. We define the desired number of particles per cell N_{ppc}. Then each particle gets its desired weight $w_{\text{d}}(i)$ according to

$$w_{\text{d}}(i) = \frac{n_{\text{s}}(i) V_{\text{cell}}}{N_{\text{ppc}}}, \tag{5}$$

   where $n_{\text{s}}(i)$ is the number density of particles of type s in the cell i and V_{cell} is the volume of a grid cell.
2. Particles with weights $w_i < 2w_{\text{d}}(i)/3$ are to be merged and particles with $w_i > 1.5w_{\text{d}}(i)$ are put to a split list.
3. We create a k–d tree according to the coordinates of the particles.
4. For particles in the **merge** list, we search the closest neighbour j of each particle i and merge them. The distance d_c to the closest neighbour is determined by

$$d_c^2 = (\vec{x}_i - \vec{x}_j)^2 + \eta^2 |\vec{v}_i - \vec{v}_j|^2, \tag{6}$$

   where η is a scaling factor that expresses the ratio of a typical length divided by a typical velocity of the charge particles [6]. We set it to 1 ps in our simulations. A newly formed particle gets its velocity at random from one of the original particles and the new weight

$$w_{\text{new}} = w_i + w_j \tag{7}$$

   is always the sum of the weights. The position of the new particle is set to the weighted average position

$$\vec{x}_{\text{new}} = \frac{w_i \vec{x}_i + w_j \vec{x}_j}{w_i + w_j}. \tag{8}$$

5. For particles in the **split** list, each particle splits into two new particles having the same position and velocity as the original particle but with a half weight $w_i/2$.

A detailed analysis of different schemes to merge particles is given in [6].

Note that for typical conditions of low pressure CCRF discharges the execution of the APM algorithm takes about 50% of the total computing time if it is executed at every time step. However, since the change of the particle numbers per cell within one time step is small for the present case of an equidistant spatial grid, the APM procedure is typically executed every 3000 time steps and thus its computational cost is negligible.

2.3. Boundary conditions for particles

Different boundary conditions for particles have to be considered in the simulation, which are determined by the discharge condition and the boundary material. Frequently, it is assumed that the fluxes of the charged particles reaching the boundaries (electrodes in our case) are completely absorbed and that secondary

Please cite this article in press as: A. Sun, et al., PIC/MCC simulation of capacitively coupled discharges: Effect of particle management and integration, Computer Physics Communications (2016), http://dx.doi.org/10.1016/j.cpc.2016.05.003

particles such as electrons are not emitted [18]. We consider a partial reflection boundary condition for all charged particles with particle-specific reflection coefficient and add secondary electrons to the discharge region if their emission is included in the discharge model.

The treatment of particles that approach the boundary is different for the two particle integration methods included. For the leapfrog particle mover, we use an algorithm similar to that present in [44]. The time t_b and velocity v_b when a particle reaches a boundary located at x_b is calculated as

$$t_b = t_k + \left| \frac{x_b - x_k}{v^x_{k-1/2}} \right|, \tag{9}$$

$$v_b = v^x_{k-1/2} + \left| \frac{x_b - x_k}{v^x_{k-1/2}} \right| a^x_k, \tag{10}$$

where a^x_k defines the acceleration in x-direction at time t_k. The velocity and position of the particle after the reflection are expressed as

$$v^x_{k+1/2} = -v_b + (t_{k+1} - t_b)a^x_k, \tag{11}$$

$$x_{k+1} = x_b - v_b(t_{k+1} - t_b) + \frac{1}{2}a^x_k(t_{k+1} - t_b)^2. \tag{12}$$

If the velocity Verlet integration method is used, the reflection of particles at a boundary becomes a bit more complex, since the acceleration a^x_{k+1} at the time t_{k+1} is needed for updating the velocity. A procedure as follows is used in the present model. Firstly, we calculate the time t_b and velocity v_b at the boundary similar to the leapfrog scheme according to Eqs. (9) and (10). Secondly, the new position of all particles after the reflection is determined according to Eq. (12). Then, the Poisson equation is solved once at the time t_{k+1} so that the acceleration a_b at the boundary and a^x_{k+1} at the new position of the particle are obtained. Finally, the velocity of the particle is determined by

$$v^x_{k+1} = -v_b + \frac{1}{2}(a_b + a^x_{k+1})(t_{k+1} - t_b). \tag{13}$$

Ions impinging onto the surface can also emit secondary electrons from the surface. These electrons are emitted isotropically into the half range in front of the boundary and are assumed to have a Maxwellian energy distribution with a mean energy of 2 eV, but limited to the interval (0, 5 eV].

2.4. Collision processes

Because of the low ionization degree in the plasmas of interest, neutral-charged particle collision processes are predominant so that only electron-neutral and ion-neutral collision processes are included in the present model. These collision processes are modelled with the MCC approach using the null-collision method [45].

For the PIC/MCC simulations of the low-pressure CCRF discharges in helium and the benchmark studies, we use the same collision cross section data as in [18]. The electron-neutral collisions include the elastic momentum transfer, two excitation processes as well as ionization leading to the generation of atomic helium ions, where isotropic scattering in the centre-of-mass frame is assumed for the collision processes. The ion-neutral collisions take into account isotropic elastic scattering as well as charge exchange following [46], both in the centre-of-mass frame. In order to take the velocity of neutral background gas particles during the collision process into account, we randomly choose a neutral velocity of the Maxwellian distribution at given gas temperature. But the motion of neutral particles is not traced and its density remains constant.

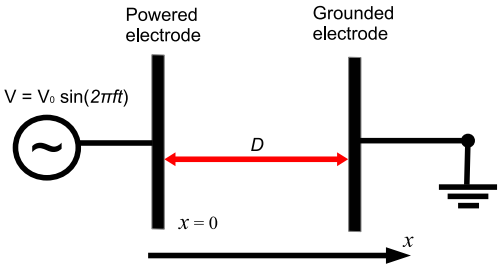

Fig. 2. Schematic of the one-dimensional, symmetric parallel-electrode RF discharge configuration.

2.5. Code parallelization

Particle models are very time-consuming due to the large amount of particles that have to be traced, although an adaptive particle management is adopted. Fortunately, PIC simulations have generally a high parallel performance for the particle movement routines. Therefore, we parallelize the code using MPI computing, where the particle population is equally shared among the processes. All calculations are performed on a modern computing cluster and the computation is around 10 times faster for $p = 13.3$ Pa (3 h vs. 31 h) and around 8 times faster for $p = 133$ Pa (3 days vs. 25 days) if we use 16 CPU cores instead of one.

3. Code verification

In this section, the developed PIC/MCC code is verified by comparing the results with benchmark simulations for a low-pressure CCRF discharge in helium reported by Turner et al. [18]. The conditions for these 1d3v PIC/MCC studies have been chosen to represent the experiments in [24]. A symmetric RF discharge between two plane-parallel electrodes is considered, where the electrodes are perpendicular to the x axis. A schematic of the discharge configuration is shown in Fig. 2. The distance between the two parallel electrodes is $D = 6.7$ cm. A sinusoidal voltage $V(t) = V_0 \sin(2\pi ft)$ with a frequency $f = 13.56$ MHz and an amplitude V_0 is applied to the powered electrode located at $x = 0$, while the other electrode located at $x = D$ is grounded.

The comparison with the benchmark results reported in [18] has been performed for four parameter conditions in the pressure range between 4 and 133 Pa at a gas temperature of 300 K. Here, results for the pressures p of 13.3 and 133 Pa are exemplarily reported. The applied voltage amplitude V_0 and the initial plasma density n_0 are 200 V and 5.12×10^{14} m^{-3} for $p = 13.3$ Pa and 120 V and 3.84×10^{14} m^{-3} for $p = 133$ Pa. The initial temperature of electrons and ions is 30 000 and 300 K, respectively. As in [18] it is assumed that the fluxes of charged particles reaching the electrodes are completely absorbed and no secondary particles are emitted. The respective number of cells and time step size is $N_x = 256$ and $\Delta t = (800f)^{-1}$ and $N_x = 512$ and $\Delta t = (3200f)^{-1}$ for $p = 13.3$ and 133 Pa, respectively. We use a number N_{ppc} of 256 for 13.3 Pa and 128 for 133 Pa, respectively, to define the desired weights according to Eq. (5) for the adaptive particle management. The number of N_{pcc} is chosen such that the accuracy of the simulation is ensured without increasing the computational cost too much. Note that the influence of N_{pcc} on the results is analysed in Section 4.1.

Fig. 3 shows a comparison between our simulations and the benchmark results [18] for the ion density n_i, the time-averaged heating rate of electrons P_e and ions P_i given by $P_{e,i} = \langle J_{e,i} \cdot E \rangle$ with the electron (J_e) and ion (J_i) current density and the electric field E in x-direction as well as for the normalized electron energy probability functions (EEPF). The leapfrog particle integration

Please cite this article in press as: A. Sun, et al., PIC/MCC simulation of capacitively coupled discharges: Effect of particle management and integration, Computer Physics Communications (2016), http://dx.doi.org/10.1016/j.cpc.2016.05.003

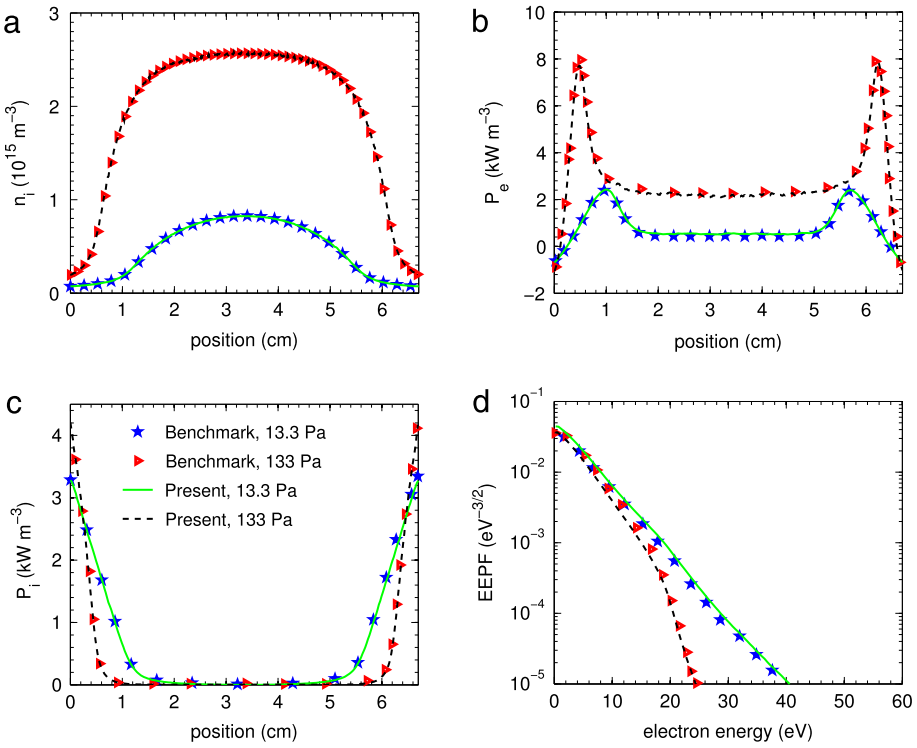

Fig. 3. Comparison of ion density (a), heating rate of electrons (b) and ions (c) and normalized electron energy probability functions (d) obtained by present simulations and the benchmark results of Turner et al. [18]. Leapfrog particle integration is used for the simulations.

Table 1
Comparison between present and benchmark results [18] for the ion density n_i and electron temperature T_e in the mid-plane of the discharge, the line integrated electrical power S_e and S_i coupled to electrons and ions, respectively, and the ion current J_i collected at either electrode.

	13.3 Pa		133 Pa	
	Present	Benchmark	Present	Benchmark
n_i (10^{14} m^{-3})	8.3	8.28	25.6	25.7
$k_B T_e$ (eV)	4.65	4.69	3.66	3.65
S_e (W m^{-2})	51.9	51.6	194	193
S_i (W m^{-2})	44.0	43.3	27.5	27.1
J_i (A m^{-2})	0.214	0.215	0.181	0.186

method is used here in order to be consistent with the reference models [18].

Very good agreement is obtained between our and the benchmark simulation results for the spatial variation of the ion density and the heating rates as well as for the normalized EEPF for the different pressures considered. In addition, main physical parameters reported in [18] are also compared and the corresponding results are summarized in Table 1. The maximum error for all parameters is less than 0.5%, which is well acceptable for particle simulations. Thus, the present 1d3v PIC/MCC model including its adaptive particle management approach can be considered to be reliable and well applicable for further studies.

4. Convergence study

In addition to the comparison with the benchmark results, the influence of the super particle numbers per cell (N_{ppc}) used for the APM algorithm described in Section 2.2 is analysed in order to ensure that the issue of not conserving momentum and energy at the same time [5,6] does not affect the accuracy of the present PIC/MCC model. Furthermore, a comparison between results obtained by using the leapfrog and the velocity Verlet integration scheme is represented focusing on the convergence behaviour of these methods with respect to the time step size.

4.1. Influence of super particle numbers per cell

Since adaptive particle management is used in the present code to adjust the weight of super particles, it has to be ensured that the results are not affected by the general issue of the present APM method of not conserving momentum and energy of super particles after merging or splitting [6]. According to the comparison of various merge schemes in [6], a scheme that selects properties for the merged particle at random from the original particles is used in our code, as stated in Section 2.2. Note that this scheme performs better than others, because it can conserve on average both momentum and energy [6]. We have shown in Section 3 that results including APM with a certain number of super particles per cell agree very well with the results of Turner et al. [18]. In this section, we investigate further how the accuracy of the simulations is affected by the chosen number of super particles by comparing with results obtained without APM for different super particle numbers. The same discharge conditions as in Section 3 are used here.

A comparison of numerical and physical quantities obtained for different N_{ppc} is shown in Figs. 4 and 5 as well as in Tables 2 and 3. Fig. 4 presents the time averaged numbers and weights of super particles (ions) obtained for different N_{ppc} as well as the super particle numbers that have been obtained without using APM for constant weights. As expected, the number of super particles increases and the averaged weight decreases with increasing N_{ppc}, see also Tables 2 and 3. It is shown in Fig. 4(a), (c) that the APM algorithm generally aims at an equal distribution of the super particles per cell over the entire computational domain. Obviously, this condition is better fulfilled for the higher pressure case (133 Pa, see Fig. 4(c)) than for the lower pressure case (13.3 Pa, see Fig. 4(a)). Note that the number of super particles is particularly increased in the sheath regions if APM is used. That is, compared to the usage of

Please cite this article in press as: A. Sun, et al., PIC/MCC simulation of capacitively coupled discharges: Effect of particle management and integration, Computer Physics Communications (2016), http://dx.doi.org/10.1016/j.cpc.2016.05.003

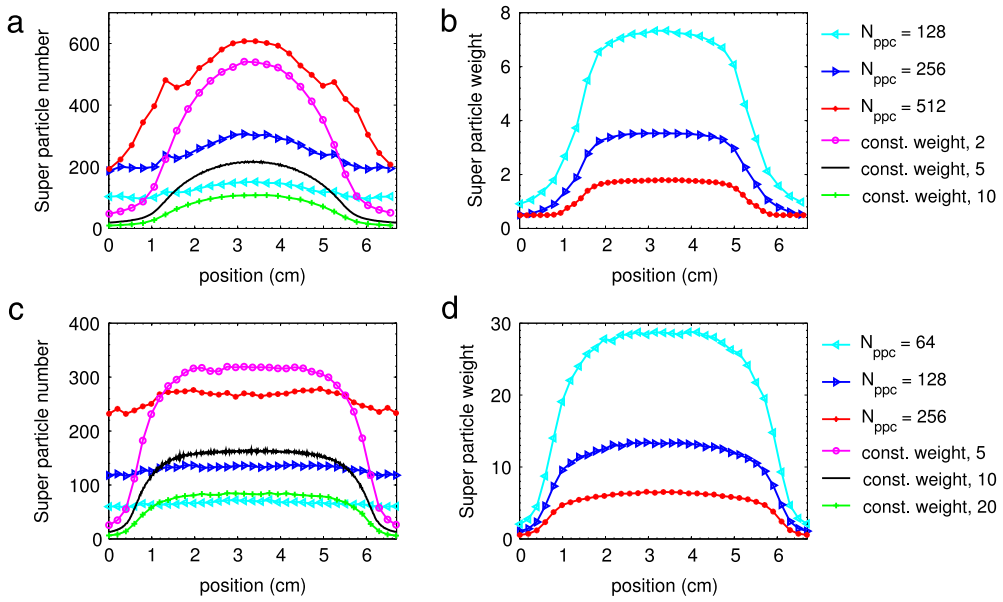

Fig. 4. Time averaged number (a), (c) and weight (b), (d) of super particles (ions) per cell as a function of position for different N_{ppc}. (a) and (b): $p = 13.3$ Pa; (c) and (d): $p = 133$ Pa. The Leapfrog particle integration method is used for the simulations.

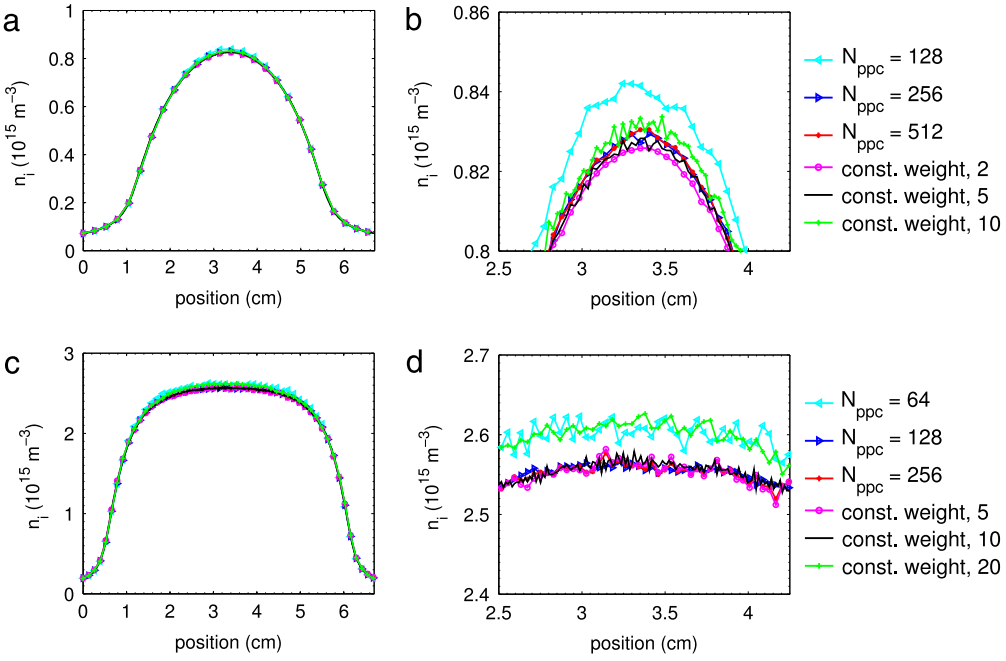

Fig. 5. Time averaged ion density as a function of position for different N_{ppc}. (a) and (b): $p = 13.3$ Pa; (c) and (d): $p = 133$ Pa. The simulation conditions are the same as in Fig. 4.

a constant particle weight, a higher accuracy is to be expected with APM at the same computational cost if boundary effects markedly influence the plasma parameters.

Fig. 5 illustrates the impact of the respectively chosen values of N_{ppc} (with APM) and particle weights (without APM) on the accuracy of the numerical solution obtained for the ion density. The exact values of the maximum ion density at the centre of the discharge region and the corresponding relative deviation from the benchmark results [18] are also listed in Tables 2 and 3. It turns out that for both pressures the obtained results converge to the reference solutions within the statistical error tolerance if N_{ppc} is chosen large enough. Converged results are obtained for $N_{ppc} = 256$ at $p = 13.3$ Pa and for $N_{ppc} = 128$ at $p = 133$ Pa. This proves that the problem of the APM algorithm of not simultaneously conserving momentum and energy does not affect the convergence of the PIC/MCC model. Note that this may no longer be valid in case that particles are merged and split at every time step because then the introduced error could become large compared to the statistical error due to accumulation effects.

A direct comparison of the relative deviations from the reference solution at the centre of the discharge as a function of the total number of super particles obtained for different values of N_{ppc} and different constant weights is presented in Fig. 6. The uncertainty ranges indicated by the error bars here are determined by running the code three times starting with different random numbers, and thus represent the intrinsic error of the PIC/MCC model due to particle fluctuations. It turns out that for $p = 13.3$ Pa the solution obtained without using the APM algorithm is

Please cite this article in press as: A. Sun, et al., PIC/MCC simulation of capacitively coupled discharges: Effect of particle management and integration, Computer Physics Communications (2016), http://dx.doi.org/10.1016/j.cpc.2016.05.003

Table 2
Effect of the desired super particle numbers per cell (N_{ppc}) on the mean weight of super particles (w_m), total number of super particles ($N_{sup,part}$), averaged maximum ion density ($n_{i,max}$) and the error ($\Delta n_{i,max}$). We define $\Delta n_{i,max} = \frac{|n_{i,max}-n_{0,max}|}{n_{0,max}}$, where $n_{0,max}$ is the maximum ion density in the benchmark [18]. Simulations are performed at $p = 13.3$ Pa with the leapfrog integration method.

N_{ppc}	$w_{m,part}$	$N_{sup,part}$	$n_{i,max}$ (10^{15} m^{-3})	$\Delta n_{i,max}$
32	19.01	8 192	0.872	5.31%
64	9.40	16 410	0.855	3.26%
128	4.60	32 461	0.841	1.57%
256	2.40	58 138	0.830	0.24%
512	1.31	119 354	0.831	0.36%

Table 3
Same as Table 2, but for $p = 133$ Pa.

N_{ppc}	w_m	$N_{sup,part}$	$n_{i,max}$ (10^{15} m^{-3})	$\Delta n_{i,max}$
32	39.08	17 525	2.755	7.20%
64	18.72	34 511	2.613	1.67%
128	9.31	67 552	2.564	0.23%
256	4.36	127 851	2.575	0.20%
512	2.30	248 763	2.576	0.23%

more accurate than the solution obtained with APM if a low total number of super particles is used. For $p = 133$ Pa the convergence behaviour with respect to the total number of super particles is almost the same with or without using APM. The increasing relevance of the APM algorithm with increasing pressure is directly connected with the physical properties of the discharge under consideration. At $p = 13.3$ the ionization processes determining the plasma density occur mainly in the bulk region [18]. Thus, the increased number of super particles in the sheath regions at the expense of fewer particles in the plasma bulk caused by the APM procedure is disadvantageous and leads to a drop of the accuracy compared to the case with a constant weight of super particles. With increasing pressure the maximum ionization rate moves towards the sheath regions [18] and the increased number of super particles in the sheath regions achieved by APM starts to be advantageous. A higher accuracy with APM than without APM for the same total number of super particles is to be expected if

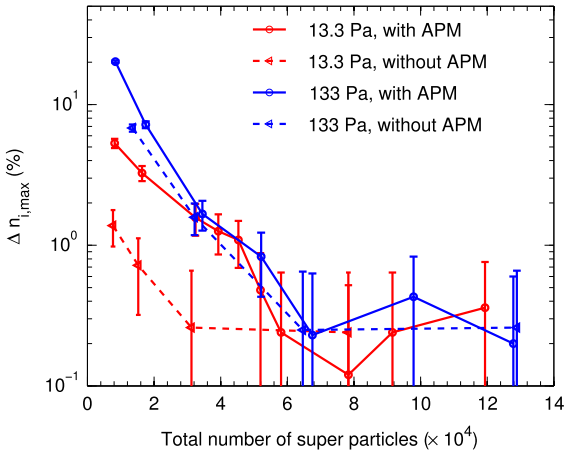

Fig. 6. Relative deviation from the reference solution as a function of the total number of super particles (ions) for different pressures with and without using APM. The error bar indicates the deviations induced by intrinsic particle fluctuations.

the plasma parameters are influenced by boundary effects like the emission of secondary electrons.

Besides its possible impact on the overall accuracy of the results provided by PIC simulations, the APM has an additional positive "side effect". The increased number of super particles in the sheath regions (cf. Fig. 4(a), (c)) allows a better determination of macroscopic quantities like, e.g., the mean electron energy which is hardly to deduce if very few electrons are present, only.

4.2. Influence of particle integration method and time step size

The present PIC/MCC code includes the velocity Verlet integration method in addition to the common leapfrog scheme used by the five different codes of the benchmark studies reported in [18]. In order to analyse the impact of both the algorithms for solving the equations of motion on the results, a number of simulations have been performed using different time step sizes.

The resulting ion density distributions for the two pressures of 13.3 and 133 Pa are represented in Fig. 7. It becomes obvious that

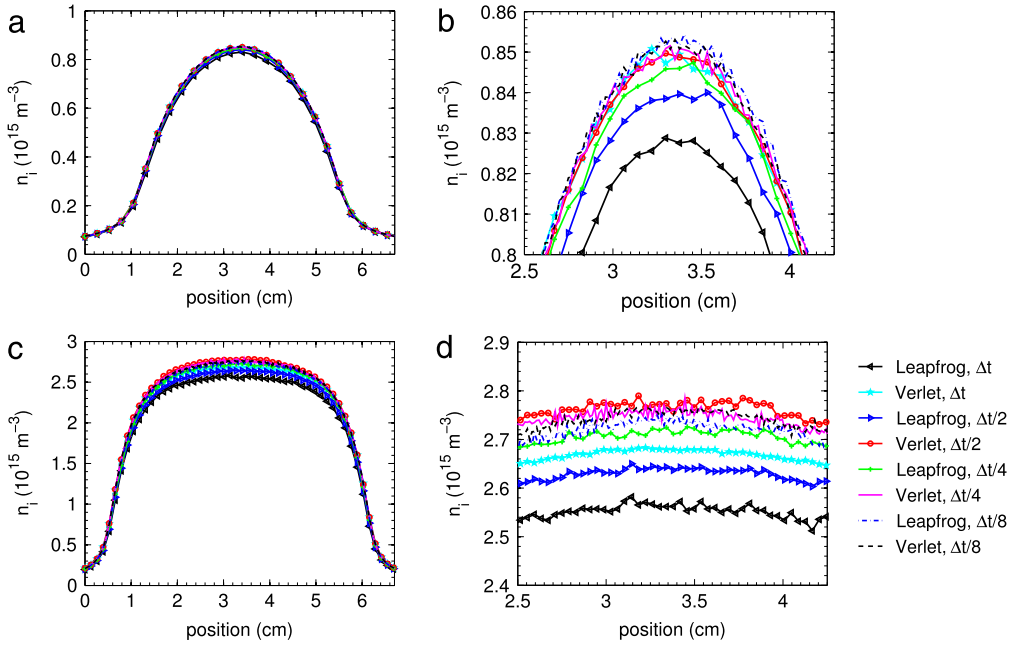

Fig. 7. Time averaged ion density as a function of position for different time step sizes, using leapfrog and velocity Verlet particle integration method. (a) and (b) with $\Delta t = (800f)^{-1}$ at $p = 13.3$ Pa, while (c) and (d) with $\Delta t = (3200f)^{-1}$ at $p = 133$ Pa.

Please cite this article in press as: A. Sun, et al., PIC/MCC simulation of capacitively coupled discharges: Effect of particle management and integration, Computer Physics Communications (2016), http://dx.doi.org/10.1016/j.cpc.2016.05.003

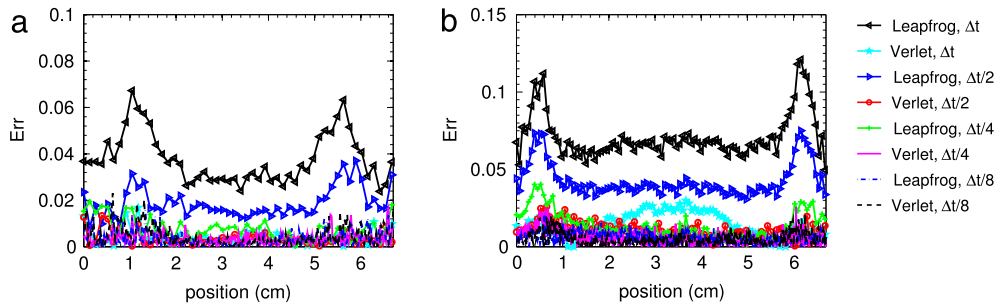

Fig. 8. Relative error as a function of position for different time step sizes, (a) for $p = 13.3$ Pa and (b) for $p = 133$ Pa. The same simulation conditions as in Fig. 7 are used.

the results obtained by the leapfrog and the velocity Verlet scheme do not agree if the standard time step size of the benchmark simulations in [18], namely $\Delta t = (800f)^{-1}$ at 13.3 Pa and $\Delta t = (3200f)^{-1}$ at 133 Pa are used. However, the results of both particle integration methods converge to the same solution if the time step size is sufficiently decreased. Furthermore, it is shown that for the standard time step sizes the results obtained by the velocity Verlet scheme are in better agreement with the converged solution for the ion density than the results obtained by the leapfrog scheme used in [18]. Note that the influence of the time step size and other numerical parameters is also briefly studied in [18]. However, we found that their refined results with a four times reduced grid size and time step do not agree with our results obtained with the smallest time step. We have also checked that the influence of a four times smaller grid is around 0.6% and is thus negligible.

In order to investigate the convergence properties of the considered particle integration schemes systematically, the relative deviation

$$\mathrm{Err}(x_j) = \frac{\left|n_\mathrm{i}(x_j) - n_\mathrm{i}^\mathrm{ref}(x_j)\right|}{n_\mathrm{i}^\mathrm{ref}(x_j)}, \tag{14}$$

of the ion density $n_\mathrm{i}(x_j)$ from the converged reference ion density obtained by a time step of $\Delta t/32$ at the position x_j is calculated.

As it is shown in Fig. 8, taking $p = 13.3$ Pa as an example (cf. Fig. 8(a)), the relative deviation of the ion density at benchmark conditions from the reference solution amounts to about 4% in the bulk plasma and up to about 6% around the sheath edge for the leapfrog method and it is generally less than 2% for the velocity Verlet scheme. For smaller time step sizes, these errors decrease at all positions for both the particle integration methods. At 133 Pa the error introduced by the leapfrog scheme at standard conditions is even higher (cf. Fig. 8(b)).

Fig. 9 shows the change of the relative error for the maximum ion density ($\Delta n_{\mathrm{i,max}}$) at the centre of the discharge domain (i.e. $j = (N+1)/2$ in Eq. (14)), with different time step sizes in the range from $\Delta t/16$ to $8\Delta t$, where $N = 257$ for 13.3 Pa and $N = 513$ for 133 Pa denotes the number of grid points. Obviously, $\Delta n_{\mathrm{i,max}}$ remains below the statistical error of about 1% for both pressures when the time step is increased by a factor of 16 from $\Delta t/16$ to Δt for the velocity Verlet scheme. At the same time $\Delta n_{\mathrm{i,max}}$ increases markedly when the leapfrog scheme is used. At the largest time step considered ($8\Delta t$) the relative error $\Delta n_{\mathrm{i,max}}$ obtained from the leapfrog scheme is one order of magnitude larger than that of the velocity Verlet scheme.

Thus, we can conclude that the velocity Verlet scheme is less sensitive to the time step size than the leapfrog scheme. This might result from the stronger coupling between particle motion integration and electric field determination caused by the use of the intermediately updated acceleration $\vec{a}_{k+1}$ in Eq. (4).

The simulations above indicate that one has to be cautious in choosing a particle integration method and appropriate time step to get almost converged results. They also show that the comparison with benchmark results requires special care if the results are not converged or different methods are used. The velocity Verlet integration method for particles appears to be more suitable for the simulation of CCRF discharge plasmas because it can keep appropriate accuracy of simulations at less computational time.

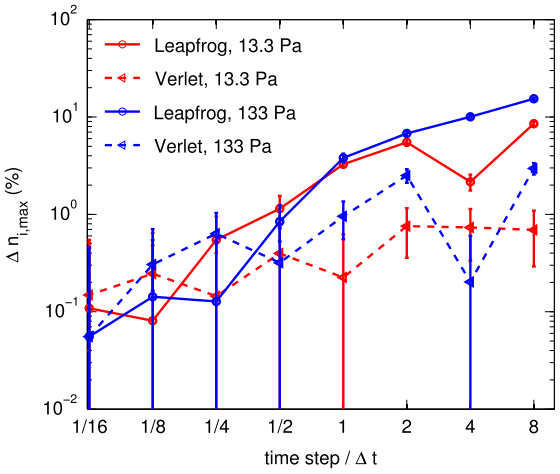

Fig. 9. Relative error of the maximum ion density at the centre of the discharge domain, for different time step sizes. The error bar indicates the deviations induced by intrinsic particle fluctuations. The same simulation conditions as in Fig. 7 are used.

4.3. Influence of the working gas

In order to verify the generality of the conclusions drawn so far regarding the applicability of the APM algorithm and the different particle integration schemes, additional simulations of a low pressure CCRF discharge in argon have been performed.

The simulation conditions are the same as those used in section 4 of Erden et al. [7]. The discharge configuration is the same as shown in Fig. 2 with a gap distance of $D = 2.5$ cm. A sinusoidal voltage $V(t) = V_0 \sin(2\pi ft)$ with $V_0 = 250$ V is applied to the powered electrode with a frequency of $f = 13.56$ MHz. In accordance with [7], the grid cell size $\Delta x = 4.17 \times 10^{-5}$ m (corresponding to 600 grid cells), and the time step size $\Delta t = 2.67 \times 10^{-12}$ s are used. The pressure and temperature of the neutral argon gas are 10 Pa and 350 K, respectively. Electron-neutral and ion-neutral collision cross sections are taken from [47] and [46], respectively. Particles reaching the electrodes are assumed to be completely absorbed and the emission of secondary electrons was neglected in order to stay consistent with the present investigations for helium. Note that in [7] the emission of secondary electrons has been taken into account.

In Figs. 10 and 11 the respective time-averaged ion densities, number and weight of super particles (ions) are shown as a function of the position obtained with and without using APM. If

Please cite this article in press as: A. Sun, et al., PIC/MCC simulation of capacitively coupled discharges: Effect of particle management and integration, Computer Physics Communications (2016), http://dx.doi.org/10.1016/j.cpc.2016.05.003

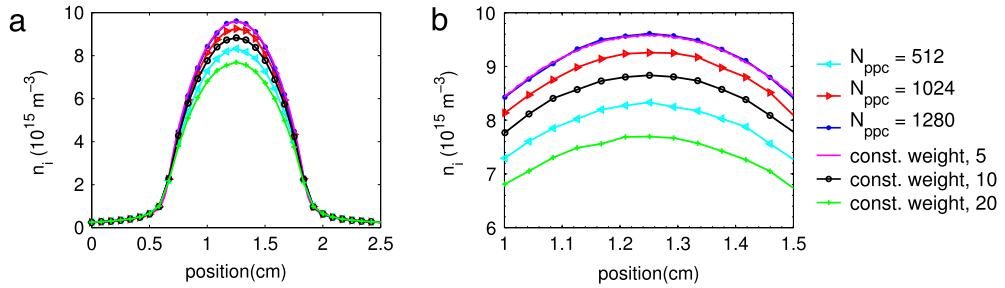

Fig. 10. Time averaged ion density as a function of position in argon for $p = 10$ Pa and $V_0 = 250$ V obtained with and without APM. The leapfrog integration method is used in the simulations.

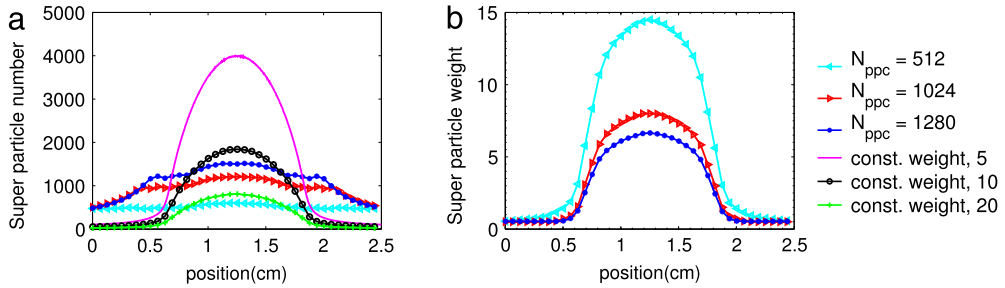

Fig. 11. Time averaged number (a) and weight (b) of super particles (ions) per cell as a function of position for different N_{ppc}. The simulation conditions are the same as in Fig. 10.

sufficient super particles are used, excellent agreement is observed between the two solutions (e.g. AMP with $N_{ppc} = 1280$ and a constant weight of 5 corresponding to approximately 1500 super particles per cell, in Fig. 10). This confirms that the parameters leading to converged results in helium (cf. Fig. 5) are applicable for similar discharge situations in argon, too. However, it was observed that the convergence in argon is more sensitive to the weight of super particles than in helium both when neglecting and including APM. Similar effects of super particle weighting on the accuracy of PIC simulations in argon have also been reported in [7].

The impact of the time step size on the relative error (14) of the maximum ion density at the centre of the discharge domain provided by the leapfrog and the velocity Verlet integration scheme for the considered CCRF discharge in argon is depicted in Fig. 12. Again, the velocity Verlet scheme appears to be less sensitive to the time step sizes and shows better convergence properties than the leapfrog scheme, in agreement with the results obtained for helium (cf. Fig. 9). Here, the error remains in an acceptable range of about 1% if the default time step Δt is increased by a factor of 16 for the velocity Verlet scheme and by a factor of 4 for the leapfrog scheme.

Additional calculations were performed for the CCRF discharge conditions investigated by Lafleur et al. [38] (section 3 of [38], argon, 66.66 Pa, 300 K). The obtained results (not shown here) confirmed the generality of the drawn conclusions regarding the particle management and the integration methods.

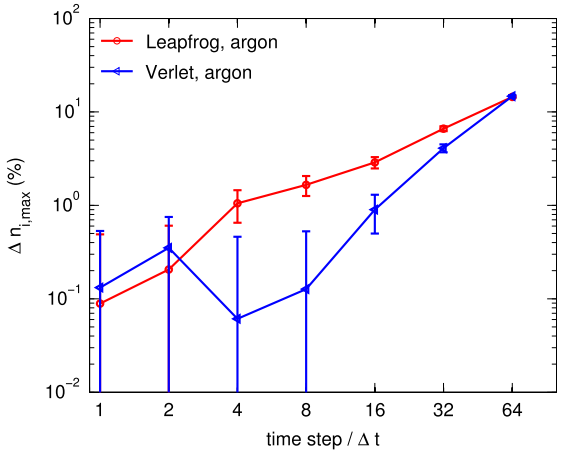

Fig. 12. Relative error of the maximum ion density at the centre of the discharge domain for different time step sizes, in argon. The error bar indicates the deviations induced by intrinsic particle fluctuations and the numerical conditions are the same as in Fig. 10.

5. Summary

A PIC/MCC code for the simulation of low-temperature gas discharge plasmas was introduced. It includes the common leapfrog and the velocity Verlet integration method for integrating Newton's equations of motion for electrons and ions, an adaptive particle management to adjust the weight of super particles and parallel computing using MPI. Main features of the simulation tool were represented and differences between the particle integration methods were discussed.

The present PIC/MCC simulation method was applied to studies of CCRF discharges in helium and argon. The comparison with corresponding benchmark simulation results reported in [18] demonstrated well the accuracy and applicability of the code. It was particularly shown that the results obtained with and without APM converge to the same solution if the number super particles per cell is large enough. It was pointed out that the application of the present APM algorithm can be disadvantageous regarding the accuracy of the model for a given total number of super particles in case that only processes in the plasma bulk determine the plasma properties and the sheath regions are of minor importance.

Furthermore, the comparison of the results obtained from the leapfrog and velocity Verlet integration method for different time step sizes suggests the use of the velocity Verlet particle integration method for the simulation of discharge plasmas because it allows for larger time step sizes than the leapfrog algorithm at appropriate accuracy of simulations. The comparative studies also pointed out that the comparison with benchmark results requires special care, if the results are not converged with respect to certain numerical parameters or different methods are employed.

Please cite this article in press as: A. Sun, et al., PIC/MCC simulation of capacitively coupled discharges: Effect of particle management and integration, Computer Physics Communications (2016), http://dx.doi.org/10.1016/j.cpc.2016.05.003

The generality of the drawn conclusions regarding the particle management and the integration methods was verified by showing that the results obtained for helium are still valid if the present PIC/MCC model is applied for the simulation of a low pressure CCRF discharge in argon.

Acknowledgements

ABS acknowledges the support of PlasmaShape project from the European Union under grant agreement no 316216. This work was additionally supported in part by German Research Foundation within the Transregional Collaborative Research Centre Transregio 24 "Fundamentals of complex plasmas" (no INST 292/44-3). The authors thank A. Derzsi, Z. Donkó and M.M. Turner very much for their kind assistance in benchmarking the code.

References

[1] K. Matyash, R. Schneider, F. Taccogna, A. Hatayama, S. Longo, M. Capitelli, D. Tskhakaya, F.X. Bronold, Particle in cell simulation of low temperature laboratory plasmas, Contrib. Plasma Phys. 47 (2007) 595–634.
[2] Z. Donkó, Particle simulation methods for studies of low-pressure plasma sources, Plasma Sources Sci. Technol. 20 (2011) 024001.
[3] G. Lapenta, J. Brackbill, Control of the number of particles in fluid and mhd particle in cell methods, Comput. Phys. Comm. 87 (2002) 139–154.
[4] F. Assous, T.P. Dulimbert, J. Segré, A new method for coalescing particles in PIC codes, J. Comput. Phys. 187 (2002) 550–571.
[5] D. Welch, T. Genoni, R. Clark, D. Rose, Adaptive particle management in a particle-in-cell code, J. Comput. Phys. 227 (2007) 143–155.
[6] J. Teunissen, U. Ebert, Controlling the weights of simulation particles: adaptive particle management using *k–d* trees, J. Comput. Phys. 259 (2014) 318–330.
[7] E. Erden, I. Rafatov, Particle in cell/Monte Carlo collision method for simulation for RF glow discharges: effect of super particle weighting, Contrib. Plasma Phys. 54 (2014) 626–634.
[8] M. Toggweiler, A. Adelmann, P. Arbenz, J.J. Yang, A novel adaptive time stepping variant of the BorisBuneman integrator for the simulation of particle accelerators with space charge, J. Comput. Phys. 273 (2014) 255–267.
[9] C.K. Birdsall, A.B. Langdon, Plasma Physics Via Computer Simulation, McGraw-Hill, New York, 1974.
[10] G.B. Jacobs, J.S. Hesthaven, Implicit–explicit time integration of a high-order particle-in-cell method with hyperbolic divergence cleaning, Comput. Phys. Comm. 180 (2009) 1760–1767.
[11] P. Degond, F. Deluzet, L. Navoret, A.B. Sun, H. Vignal, Asymptotic-preserving particle-in-cell method for the vlasov–Poisson system near quasineutrality, J. Comput. Phys. 229 (2010) 5630–5652.
[12] O. Chanrion, T. Neubert, A PIC-MCC code for simulation of streamer propagation in air, J. Comput. Phys. 227 (2008) 7222–7245.
[13] T. Hemke, D. Eremin, T. Mussenbrock, A. Derzsi, Z. Donkó, K. Dittmann, J. Meichsner, J. Schulze, Ionization by bulk heating of electrons in capacitive radio frequency atmospheric pressure microplasmas, J. Phys. D: Appl. Phys. 22 (2013) 015012.
[14] A.B. Sun, J. Teunissen, U. Ebert, The inception of pulsed discharges in air: simulations in background fields above and below breakdown, J. Phys. D: Appl. Phys. 47 (2014) 445205.
[15] J. Teunissen, A.B. Sun, U. Ebert, A time scale for electrical screening in pulsed gas discharges, J. Phys. D: Appl. Phys. 47 (2014) 365203.
[16] R.W. Hockney, J.W. Eastwood, Computer Simulation Using Particles, IOP Publishing, Bristol, 1988.
[17] W.C. Swope, H.C. Andersen, P.H. Berens, K.R. Wilson, A computer simulation method for the calculation of equilibrium constants for the formation of physical clusters of molecules: Application to small water clusters, J. Chem. Phys. 76 (1982) 637–649.
[18] M.M. Turner, A. Derzsi, Z. Donkó, D. Eremin, S.J. Kelly, T. Lafleur, Simulation benchmarks for low-pressure plasma: capacitive discharges, Phys. Plasmas 20 (2013) 013507.
[19] M.A. Liberman, A.J. Lichtenberg, Principles of Plasma Discharges and Materials Processing, Wiley Interscience, New York, 2005.
[20] D.M. Manos, D.L. Flamm, Plasma Etching, Academic, New York, 1989.
[21] T. Makabe, Z. Petrovic, Plasma Electronics: Applications in Microelectronic Device Fabrication, Taylor & Francis, 2006.
[22] T.V. Woedtke, S. Reuter, K. Masur, K.D. Weltmann, Plasmas for medicine, Phys. Rep. 530 (2013) 291–320.
[23] V.A. Godyak, R.B. Piejak, B.M. Akexandrovich, Evolution of the electron energy distribution function during RF discharge transition to the high-voltage model, Phys. Rev. Lett. 68 (1992) 40–43.
[24] V.A. Godyak, R.B. Piejak, B.M. Akexandrovich, Measurement of electron energy distribution in low-pressure RF discharges, Plasma Sources Sci. Technol. 1 (1992) 36–58.
[25] I.V. Schweigert, V.A. Schweigert, Combined PIC-MCC approach for fast simulation of a radio frequency discharge at a low gas pressure, Plasma Sources Sci. Technol. 13 (2004) 315–320.
[26] V. Vahedi, C.K. Birdsall, M.A. Liberman, G. Dipeso, T.D. Rognlien, Capacitive RF discharges modelled by particle-in-cell Monte Carlo simulation. II: comparisons with laboratory measurements of electron energy distribution functions, Plasma Sources Sci. Technol. 2 (1993) 273–278.
[27] F.X. Bronold, K. Matyash, D. Tskhakaya, R. Schneider, H. Fehske, Radio-frequency discharges in oxygen. I: Modeling, J. Phys. D: Appl. Phys. 40 (2007) 6583.
[28] C. Küllig, K. Dittmann, T. Wegner, I. Sheykin, K. Matyash, D. Loffhagen, R. Schneider, J. Meichsner, Dynamics and electronegativity of oxygen RF plasmas, Contrib. Plasma Phys. 52 (2012) 836–846.
[29] O. Kalentev, K. Matyash, J. Duras, K.F. Lüskow, R. Schneider, N. Koch, M. Schirra, Electrostatic ion thrusters—towards predictive modeling, Contrib. Plasma Phys. 54 (2014) 235–248.
[30] A. Hatayama, Progress in modeling and numerical simulation of negative hydrogen ion sources, Rev. Sci. Instrum. 79 (2008) 02B901.
[31] F. Iza, J.K. Lee, M.G. Kong, Electron kinetics in radio-frequency atmospheric pressure microplasmas, Phys. Rev. Lett. 99 (2007) 075004.
[32] J.P. Verboncoeur, M.V. Alves, V. Vahedi, C.K. Birdsall, Simultaneous potential and circuit solution for 1d bounded plasma particle simulation codes, J. Comput. Phys. 104 (1993) 321–328.
[33] J.T. Gudmundsson, E. Kawamura, M.A. Liberman, A benchmark study of a capacitively coupled oxygen discharge of the oopd1 particle-in-cell Monte Carlo code, Plasma Sources Sci. Technol. 22 (2013) 035011.
[34] S. Huang, J.T. Gudmundsson, A particle-in-cell/Monte Carlo simulation of a capacitively coupled chlorine discharge, Plasma Sources Sci. Technol. 22 (2013) 055020.
[35] R. Lafleur, J.P. Booth, Frequency dependence of the electrical asymmetry effect in dual-frequency capacitively coupled discharges, Appl. Phys. Lett. 102 (2013) 154104.
[36] R. Lafleur, J.P. Booth, Control of the ion flux and ion energy in CCP discharges using non-sinusoidal voltage waveforms, J. Phys. D: Appl. Phys. 45 (2012) 395203.
[37] R. Lafleur, P. Chabert, J.P. Booth, Electron heating in capacitively coupled plasmas revisited, Plasma Sources Sci. Technol. 23 (2014) 035010.
[38] R. Lafleur, P. Chabert, J.P. Booth, Electron induced asymmetry in capacitively coupled plasmas, J. Phys. D: Appl. Phys. 46 (2013) 135201.
[39] A. Derzsi, I. Korolov, E. Schüngel, Z. Donkó, J. Schulze, Effects of fast atoms and energy-dependent secondary electron emission yields in PIC/MCC simulations of capacitively coupled plasmas, Plasma Sources Sci. Technol. 24 (2015) 034002.
[40] A. Derzsi, Z. Donkó, J. Schulze, Coupling effects of driving frequencies on the electron heating in electronegative capacitive dual-frequency plasmas, J. Phys. D: Appl. Phys. 46 (2013) 482001.
[41] I. Korolov, Z. Donkó, U. Czarnetzki, J. Schulze, The effect of the driving frequencies on the electrical asymmetry of dual-frequency capacitively coupled plasmas, J. Phys. D: Appl. Phys. 45 (2012) 465205.
[42] R.A. Lippert, K.J. Bowers, R.O. Dror, M.P. Eastwood, B.A. Gregersen, J.L. Klepeis, I. Kolossvary, D.E. Shaw, A common, avoidable source of error in molecular dynamics integrators, J. Chem. Phys. 126 (2007) 046101.
[43] R. Courant, K. Friedrichs, H. Lewy, Über die partiellen Differenzengleichungen der mathematischen Physik, Math. Ann. 100 (1) (1928) 32–74. http://dx.doi.org/10.1007/BF01448839.
[44] D. Tskhakaya, K. Matyash, R. Schneider, F. Taccogna, The particle in cell method, Contrib. Plasma Phys. 47 (2007) 563–594.
[45] K. Nanbu, Probability theory of electron-molecule, ion-molecule, molecule-molecule and Coulomb collisions for particle modeling of materials processing plasmas and cases, IEEE Trans. Plasma Sci. 28 (2000) 971–990.
[46] A.V. Phelps, The application of scattering cross sections to ion flux models in discharge sheaths, J. Appl. Phys. 76 (1994) 747–753.
[47] A.V. Phelps, Z.L. Petrović, Cold-cathode discharges and breakdown in argon: surface and gas phase production of secondary electrons, Plasma Source Sci. Technol. 8 (1999) R21.